Published in final edited form as:
Small. 2011 January 17; 7(2): 242–251. doi:10.1002/smll.201001518.

Nanomaterials can Dynamically Steer Cell Responses to Biological Ligands

Dr. Ram I. Sharma,
Department of Chemical & Biochemical Engineering, Rutgers University, 98 Brett Road, NJ 08854 (USA)

Dr. Jean E. Schwarzbauer, and
Department of Molecular Biology, Princeton University, Schultz Lab, Princeton, NJ 08544 (USA)

Dr. Prabhas V. Moghe[*]
Department of Chemical & Biochemical Engineering, Rutgers University, 98 Brett Road, NJ 08854 (USA), Department of Biomedical Engineering, Rutgers University, 599 Taylor Road, Piscataway, NJ 08854 (USA)

Prabhas V. Moghe: moghe@rci.rutgers.edu

Abstract

Traditional tissue regeneration approaches to activate cell behaviours on biomaterials rely on the use of extracellular matrix based or soluble growth factor cues. In this article, we highlight a novel approach to dynamically steer cellular phenomena such as cell motility based on nanoscale substratum features of biological ligands. Albumin derived nanocarriers (ANCs) of variable nanoscale size features were functionalized with fibronectin III9–10 matrix ligand and effects on primary human keratinocyte activation were investigated. The display of fibronectin fragment from ANCs significantly enhanced cell migration compared to free ligands at equivalent concentrations. Notably, cell migration was influenced by the size of underlying ANCs even for variably sized ANCs presenting comparable levels of fibronectin fragment. For equivalent ligand concentrations, cell migration on the smaller-sized ANCs (30 nm and 50 nm) was significantly more enhanced compared to that on larger-sized ANCs (75 nm and 100 nm). In contrast, the enhancement of cell migration on nanocarriers was abolished by the use of immobilized biofunctionalized ANCs, indicating that "dynamic" nanocarrier internalization events underlie the role of nanocarrier geometry on the differential regulation of cell migration kinetics. Uptake studies using fluorescent ANCs indicated that larger-sized ANCs showed delayed endocytic kinetics and hence could present barriers for internalization during the cell adhesion and motility processes. Motile cells exhibited diminished migration upon exposure to clathrin-inhibitors, but not caveolin-inhibitors, suggesting the role of clathrin-mediated endocytosis in facilitating cell migratory responsiveness to the nanocarriers. Overall, a monotonic relationship was found between the degree of nanocarrier cytointernalization rate and cell migration rate, suggesting the possibility of designing biointerfacial features for dynamic control of cell migration. Thus, the major findings of this study are that (a) the presentation of a biorelevant ligand on a mobile nanocarrier can be used to sensitize cellular motility activation to the adhesion ligands; and (b) such nanocarrier interfaces can dynamically attune cell migration kinetics by "modulating" the uptake of the ligand-nanocarrier complex via nanocarrier size.

[*]Corresponding author.

Keywords

nanocomposites; cell motility; nanobiotechnology; biological interfaces

1. INTRODUCTION

Engineered interfaces have been designed to study cell migration based on extracellular matrix composition and structure.[1–7] Ligand chemistry, density, and presentation can govern cell migration properties.[8] The role of various adhesive ligands on cell motility behavior has been examined,[9–11] identifying motogenic ligands for the respective cell types studied and showing that for a given range of ligand concentrations, the maximum migration rate is achieved at an intermediate level of ligand. Studies examining the role of surface chemistry showed that adjusting the hydrophobicity/hydrophilicity resulted in altered ligand conformations and engendering altered cell migration.[12–14] More recently, interfaces are studied by looking at the differential organization of ligands by altering the local presentation into clusters, islands, spacing between ligands or presentation onto carriers.[15–18] These accounts demonstrate that the ligand spatial presentation at the nanoscale level could regulate cell motility, and that ligand presentation on a dynamic interface could further enhance cell motility.

Cell motility is a highly dynamic and spatially and temporally coordinated process, of significance for tissue repair, wound healing, cancer metastasis, and inflammation. The classical view of cell migration is that it results from the attachment/detachment kinetics of specific cell surface receptors with ligands of the extracellular matrix.[19] A number of ligand properties have been shown to affect cell motility, including ligand concentration, ligand-receptor adhesion strength, receptor occupancy by the ligand and ligand affinity.[9] However, cell interactions underlying motility in vivo, particularly during active wound repair and tissue regeneration, are dynamic and complex. For example, matrix molecules elicit receptor-mediated cell binding and adhesion, but are actively endocytosed, causing further cell signaling.[20,21] The utility of nanoparticles as tools to investigate and modulate interactions between integrins, cell, and extracellular matrix ligands for the control of cell adhesion and motility processes is now being realized, and nanoscale biointerfaces can be designed to emulate such interactions and, in turn, offer new approaches to control cell motility, the focus of the current investigation.

Previously, we reported that cell-binding fragments of fibronectin on nanoparticles enhanced migration of cells[22] and promoted cell contractility and extracellular matrix assembly.[23] In these studies, albumin derived nanocarriers (abbreviated ANC) were functionalized with recombinant fragments of fibronectin (abbreviated FNf), and we examined changes in the adhesion and motility behavior of primary human skin epidermal cells, keratinocytes. Using a fixed concentration of nanocarrier-derivatized fragments adsorbed onto polystyrene substrates, ligand nanodisplay enhanced cell migration. In the previous studies, we used a combination of biochemical and biophysical techniques to examine how the nanoscale display of ligands altered ligand cell-binding domain exposure. These studies showed that there was an increase in cell binding domain exposure as the carrier size increased. In the present study, we examined the role of carrier size and its mobility on cell migration while varying the ligand density.

In the current study, we have examined the role of nanoscale substrates presenting matrix ligands that activate cell motility. Substrates were adsorbed with variably sized (30–100 nm) ANCs functionalized with different concentrations of FNf (see Figure 1). The fragment includes the 10th type III domain, which houses the RGD tripeptide adhesion motif[24,25]

essential for receptor binding and concomitant signal transduction events, as well as the neighboring 9th type III domain, which contributes synergistic enhancement of integrin binding and signaling.[26–31] Here we show that ligand nanodisplay significantly enhanced cell migration rates. We first characterized the nanocarriers by quantifying the levels of FNf presented on differentially sized nanocarrier surfaces. Equal amounts of FNf were adsorbed on substrates to examine the role of ANC size on cell morphology, motility, and uptake behavior of keratinocytes. The size of ligand-nanocarriers is a critical determinant of cell motility on dynamic interfaces, as it can alter uptake kinetics. These results illustrate the potential of nanotechnology and nanobiomaterials for design of biologically-inspired dynamic cell-surface interfaces to realize improved levels of cell activation.

2. RESULTS

2.1 Surface characterization of Biofunctionalized Albumin Nanocarrier Substrates

Albumin-nanocarriers (ANCs) were fabricated by denaturing albumin monomers and stirring the suspension to generate nanocarriers by self-assembly, filtered to remove particulates greater than 200 nm, and purified via dialysis to remove monomeric albumin. A range of sizes (30–120 nm) with narrow size distributions as indicated by dynamic light scattering(Figure 2A)were created. Based on these findings, we chose to work with 30, 50, 75, and 100 nm sized ANCs. We held the mass of ANCs constant while increasing the amount of FNf added to each conjugation reaction to create a family four different preparations for each nanocarrier size.

Carriers were reacted with (*N*-succinimidyl 3-[2-pyridyldithio]-propionate) (SPDP) to introduce pyridyl disulfide (PD) groups in place of surface amino groups, making the carriers reactive to thiol groups. Recombinant protein fragments were conjugated to the surface of the nanocarrier by first displacing the amino group with SPDP, then introducing a thiol group by displacing the newly added PD group on the ligand with dithiothreotol (DTT). The newly formed thiol-containing ligand and reactive carrier were then incubated together to functionalize the ligand to the carrier. We characterized the extent of ligand conjugation as well as albumin concentration using immunosorbance techniques. By probing the GST tag on the recombinant fibronectin fragment for the ligand, we found that the extent of conjugation did not significantly differ for nanocarriers of different sizes, and nanosubstrate size did not influence ligand density (Figure 2B). Increasing the ligand amount resulted in a proportionate increase in the levels of ligand conjugated to the surface of the carrier. In order to normalize the amount of albumin adsorbed with differentially sized nanocarriers, ELISAs were also performed in parallel for the same adsorption conditions, and indicate that equal amounts of albumin are adsorbed to the surface of well plates, regardless of ligand density and carrier size (Figure 2C).

We characterized cell binding domain (CBD) exposure using immunosorbance assays by adsorbing equivalent amounts of ligand determined from isotherms for ligand-adsorbed substrates and on functionalized nanocarriers of different sizes and ligand loadings. These studies indicated that ligand exposure for a given ligand concentration was not markedly altered by nanocarrier size, however the nanocarrier-based presentation of the ligand enhanced ligand exposure compared to that of non-nanocarrier based, ligand adsorbed substrates (Figure 2D).

2.2 Cellular Morphological Responsiveness to Ligand-Nanocarriers

To characterize the effect of differential nanoparticle display of ligand on early cellular response, cell morphology was examined after 5 hours of culture. Cytoskeletal morphology was examined by staining cells for F-actin. Cells cultured on functionalized nanocarriers

exhibit filopodia-like extensions and very few stress fibers (Figure 3A–D). The degree of membrane activity seems to vary going from smallest ANC size (30 nm, Figure 3A) to largest ANC size (100nm, Figure 3D). In contrast, cells cultured on ligand-adsorbed control substrates appear to have well defined stress fibers (Figure 3E). As migratory cells are characterized with a circular shape, we analyzed the circularity of the cells on different sized nanocarriers (Figure 3F). The circularity, which measures the ratio of the area to the squared perimeter, approached 1 (a perfect circle) as the size of the carrier increased, suggesting that keratinocytes cultured on smaller sized carriers are likely more migratory.

2.3 Cell Motility Responsivness to Ligand Nanocarrier Substrates

We examined single cell motility kinetics on different sized nanocarriers while varying the ligand density. Wells were adsorbed with equivalent net quantities of ligand, either adsorbed directly to surface (controls) or conjugated to the nanocarriers, or with unfunctionalized, ligand-deficient nanocarriers. Cells were seeded, images acquired overnight, and analyzed to determine the cell speed. Cells exhibited higher levels of migration on smaller sized functionalized nanocarriers compared to larger sized nanocarriers (Figure 4A). As the ligand concentration increased, so did the levels of motility, and the trends exhibited at lower levels of migration were sustained. On ligand-adsorbed substrates cells exhibited much reduced levels of migration compared to ligand-functionalized substrates. Minimal levels of cell motility were seen on unfunctionalized substrates. Cell migration was plotted against cell binding domain exposure based on various substrate conditions (ligand versus ligand-functionalized nanocarriers), showing that increased cell binding domain exposure alone was likely not sufficient to correlate with higher rates of migration; nanoscale presentation and geometry were found to further underlie these variations (Figure 4B).

To elucidate mechanisms by which ligand-functionalized nanocarriers enhance cell motility, we cultured cells on immobilized substrates and in the presence of uptake inhibitors (Figure 4C). Oxygen plasma treatment was used to immobilize ligand-nanocarriers by introducing oxygen radicals on the substrates that cause proteins/nanocarriers to be bound to the substrate. Cells on immobilized ligand/ANCs exhibited a significant reduction in cell motility, indicating the importance of ligand/ANC dynamics underlying cell migration. Further, incorporation of clathrin uptake inhibitors reduced motility while caveolin inhibitors did not. Thus, overall cell migration was enhanced by dynamic cell-ligand/ANC interactions, which were mediated by clathrin-based uptake of ligand-ANCs.

2.4 Internalization kinetics of ligand-ANCs

The cell internalization kinetics of fluorescent ANCs was quantified by incorporation of trypan blue, added as a fluorescent quencher. Readings were taken on a fluorescent plate reader, detecting fluorescence of only internalized ligand-nanocarriers. Higher levels of ligand/ANC uptake were reported on smaller sized ligand-ANCs, with minimal uptake on immobilized substrates and reduced uptake when the cells were cultured with clathrin uptake inhibitors (Figure 5A). Cells treated with caveolin uptake inhibitors showed no reduction in uptake compared to untreated cells.

The uptake data was then used to evaluate possible correlations between cell migration kinetics and uptake rate based on overall carriers (Figure 5B) and uptake rates based on estimated ligands (Figure 5C). Figure 4B illustrates the uptake rate of ANCs appeared to more “globally” govern the kinetics of cell motility. Here, the smaller sized carriers elicited higher levels of motility and uptake while larger carriers corresponded to lower motility and uptake rates. Correlations between cell speed and estimated ligand uptake rate showed divergent profiles for different sized carriers – the smallest 30nm ANCs showed the most

sensitive effects of uptake, while the larger 100nm ANCs showed less pronounced responsiveness of cell motility to ligand uptake.

2.5 Molecular investigations of JNK activity

The MAP kinase JNK is involved in both cell motility and uptake; therefore we assayed phosphorylated JNK activity in cells on ligand-adsorbed and ligand-ANC substrates. Colorimetric ELISAs were performed to quantify phosphorylated levels of JNK on three conditions of ligand-nanocarriers: immobilization (to examine ligand binding), clathrin inhibition (to examine the contribution of uptake), and passive adsorption. Similar to motility studies, phosphorylated JNK levels were higher on smaller sized ligand-ANCs compared to larger sized ones (Figure 6A). Culturing cells with inhibitors of clathrin-mediated uptake reduced levels while immobilizing substrates further reduced JNK activity. When motility and JNK activity were plotted against each other, a monotonic correlation (R^2=0.96) was observed(Figure 6B).

3. DISCUSSION

Using substrates based on ligand-functionalized albumin nanocarriers, we report that the nanoscale presentation of matrix ligands can markedly shift cellular motility dynamics, switching motility activation from a “static” thermodynamic limitation to a “dynamic” kinetic sampling based activation. Two key implications emerge from our study: first, by activating a different cell mediated process, nanobiomaterials can be harnessed to yield high levels of cell motility unachievable on equivalent levels of ligand; second, cell motility could be tuned at different ligand concentrations by virtue of the alteration of ligand biomaterial dimensions. The net consequence is that nanoscale display of ligands on mobilizable carriers contributed toward increased biological uptake of the ligands, which correlated with enhanced cell motility, resulting from the combination of controlled nanoscale presentation of biological signals and engineered cellular remodeling processes to sample such signals. Smaller nanoscale substrates, increased matrix ligand concentration and cell-mediated internalization of the carriers were three components that accelerated the uptake dynamics as well as cell migration.

The cell adhesion and migration behavior on ligand-ANCs were manifested even at early times upon cell exposure to differently sized ANCs. On all FNf-ANC substrates, cell exhibited filopodial extensions; on smaller (30 and 50 nm) nanocarriers, filopodial extensions showed a polarized distribution that was not evident in cells on larger ANCs (75 and 100 nm), which may underlie the differential motility kinetics observed at later times. In contrast, cells on controls (FNf directly adsorbed onto the substrate) exhibited stress fibers indicative of a more stationary phenotype, and lacked the more transient filopodia.

We examined single cell motility across conditions with equivalent net amounts of ligand per area, either adsorbed directly to the surface or conjugated to nanocarriers. Cells cultured on smaller sized nanocarriers (30–50 nm) exhibited higher levels of cell migration compared to larger sized nanocarriers (75–100 nm), suggesting that motility could be tuned/regulated by alteration of substrate nanoscale dimensions. Cells migrating on ligand-adsorbed substrates exhibited a classical, biphasic motility rate behaviour:[9] the highest rate of motility was achieved at 2.5 $\mu g/cm^2$ of FNf and beyond this the rate dropped. Cell migration values on ligand-nanocarrier substrates were significantly higher than those on nanocarrier deficient ligand controls. Moreover, the cell responses showed progressive increase in migration with ligand concentration and did not exhibit a biphasic behavior. Differential cell binding domain (CBD) availability of the ligand could potentially govern the keratinocyte migration responses.[32] Plotting the cell migration rate against the corresponding CBD availability for the given substrate condition showed that increased CBD availability could

have somewhat contributed to increased cell migration, however the dynamic cell-ANC interactions and nanoscale geometry of ligand presentation were additional dominant regulators of cell migration.

To examine the mechanism by which ligand-ANCs affect cell migration, we explored the possible role of ANC dynamics in two ways. First, ligand-nanocarriers were chemically immobilized to the substrates and second, inhibitors of endocytosis were added to assess ANC uptake effects on migration. Nanocarrier mobility and subsequent endocytosis was necessary for migration, as immobilized substrates elicit diminished migration. Cell migration was compromised with the clathrin inhibitor chlorpromazine, which inhibits uptake via clathrin coated pits, indicating a role for ANC uptake mediated by clathrin endocytic mechanisms. Treatment with filipin, a caveolin inhibitor, prior to deposition on substrates, had minimal effect on migration. Thus clathrin mediated uptake is a primary mechanism for cellular sequestration and internalization of ligand-functionalized nanocarriers during cell migration on these substrates. Our studies on the kinetics of uptake confirmed active internalization of ligand-nanocarriers and variations in uptake with smaller-sized carriers endocytosed at faster rates. Given the reports that particle sizes are a determinant of nanocarrier uptake,[33] we propose that time constant for cell membrane to wrap around nanoscale carriers, t_w, may vary directly with R^2 (R=characteristic size scale) for our largely spherical nanoparticles;[34] therefore larger carriers could pose as a barrier to internalization and diminished uptake dynamics. A recent study reports that uptake is most efficient between 25 and 50 nm,[35] consistent with our observation for the smaller nanocarriers, and supports the notion that prolonged receptor binding at the cell membrane elicited by larger nanocarriers may delay complex wrapping and uptake. Additionally, a finite receptor (integrin) density may limit the kinetic sampling by cells of the underlying substrate,[36] and a time-lag in integrins readily available for re-insertion at the leading edge of the cell could likely further reduce sampling. Others have shown that internalization of matrix ligands, mediated through integrin receptors, can promote receptor recycling and cell migration.[37,38]

Nanoscale display of ligands on endocytosable carriers contributed toward increased biological uptake of the ligands, which correlated with enhanced cell migration. When cell migration rate was plotted against nanocarrier uptake rate, higher rates of migration corresponded to higher uptake rates. The highest levels of cell migration result from the combination of engineered ligand presentation via smaller nanoscale substrates and cell-mediated internalization. To determine if the ligand coverage was greater on smaller carriers and allowed for greater uptake and migration, we estimated the ligand coverage based on nanoscale geometry (Supplementary Information: Table 1), and estimated the theoretical uptake rate of ligand, which we plotted against cell migration. More ligand appears to be endocytosed via larger carriers, due to greater levels of ligands presented from these carriers. While higher rates of migration are achieved with smaller particles less ligand is taken up; furthermore four different trend regions were established as a function of nanocarrier size, further supporting the idea that nanoscale geometry was the primary and limiting determinant of cell migration rates. A small shift in ligand uptake yielded more pronounced changes in migration rates in cells cultured on smaller carriers. Based on our observations, we can conclude that the ligand-nanocarrier uptake is the rate limiting step, with the nanocarrier size being a final determinant of cell migration rate on dynamic interfaces.

The role of nanoparticle size on both endocytosis and migration indicates a significant involvement of intracellular cytoskeletal dynamics.[39] Phosphorylation of c-Jun amino-terminal kinase (JNK) has been implicated in both rapid migration on substrates with labile adhesions and uptake.[40,41] Therefore, JNK phosphorylation was assayed in cells on ligand-nanocarriers with various treatments. Phospho-JNK levels were highest in cells on

30–50 nm FNf-ANCs whereas minimal levels of phosphorylated phospho-JNK were detected on immobilized substrates. Levels of active JNK correlated with migration speed. Furthermore, active JNK was significantly reduced with addition of clathrin inhibitors. Together these results suggest that JNK signaling is a critical link between migration and endocytosis. JNK mediates migration by phosphorylating paxillin, that allows for association with focal adhesion kinase (FAK).[42,43] Inhibition of JNK activity resulted in decreased uptake in various cell lines,[44,45] but the exact mechanisms are yet to be elucidated. We believe that the internalization ligand through nanocarrier uptake is likely an insufficient signal to activate migration, as our migration studies with media supplemented ligand-ANCs, as opposed to substrate adsorbed ligand-ANCs, did not elicit enhanced migration (Supplementary Information: Table 2). Thus, the combination of ligand-nanocarrier internalization and integrated presentation through cell adhesion processes appear requisite to support enhanced migration on these interfaces.

4. CONCLUSIONS

We have investigated albumin nanocarrier based biointerfaces that present biological adhesion ligands for dynamic control of cell migration in a nanoscale attunable manner. Dynamic interfaces, such as the one we describe here, could offer an advantage for the keratinocytes specifically, and epithelial cells in general through (i) their ability to internalize matrix factors; and (ii) upregulation of signaling elements common to clathrin-mediated endocytosis and cell migration. The biocompatibility of these protein-based nanocarriers makes them viable options for exploring in vivo applications such as for enhanced re-epithelialization during treatment of wounds and skin burns, or for endocytosis-coupled motility of neural or mesenchymal stem cells in tissue regeneration scenarios.

5. METHODS

Preparation, Purification, and Characterization of Albumin Nanocarriers

Albumin nanocarriers (ANCs) were fabricated as previously described by us [22] and summarized in Figure 1. Briefly, human serum albumin (Sigma, St. Louis, MO) was diluted to 1% with phosphate-buffered saline (PBS), and filtered. The solution was subjected to a series of pH and temperature changes that allow the albumin monomers to denature. The denatured albumin solution was stirred to allow self-assembly of ANCs over different times until aggregation was stopped by incubation with 0.1% (w/v) iodoacetamide (Sigma) for 1 hour at room temperature. Monomeric albumin (66 kDa) was removed by dialysis (MWCO 100 kDa), and albumin aggregates larger than 200 nm were removed by passage through a 0.2 μm filter. The yield of ANCs was determined by performing a BCA assay on the harvested sample. To yield ANCs of different nanoscale sizes, samples were taken at various time points between 5 and 20 mniutes of stirring at 37°C and analyzed by dynamic light scattering on a PSS Nicomp 380 (Santa Barbara, CA) submicron particle sizer instrument with an argon ion laser at 532 nm.

Recombinant Protein Production and Purification

Fibronectin cDNA encoding the repeats III_9 and III_{10} were cloned for expression as a glutathione-S-transferase (GST) fusion protein. *Escherichia coli* cells were transformed with the GST-$FNIII_{9–10}$ construct and fusion proteins separated from bacterial lysates by glutathione-sepharose affinity chromatography (GE Healthcare Piscatway, NJ) following the manufacturer's recommendations. Purity of the preparations were confirmed by SDS-PAGE and Coomassie staining (Bio-Rad Laboratories). GST-$FNIII_{9–10}$ fragments were stored at −20°C and thawed immediately before use.

Preparation of Ligand-Conjugated Albumin Nanocarriers

Conjugation of the GST-FNIII$_{9–10}$ fragment to the nanocarrier was accomplished using N-succinimidyl 3-(2-pyridyldithio)propionate (SPDP) (Sigma) as previously described by us.[22] GST-FNIII$_{9–10}$ fragment and the nanocarriers of various sizes were both separately reacted with SPDP. The by-products of the reaction were removed by dialysis (MWCO 6 kDa). Next, dithiothreitol (DTT) was added to FNf, and the thiolated ligand (ligand-SH) was purified from excess DTT by dialysis. Total protein recovered from dialysis was quantified for both the nanosubstrate and the GST-FNIII$_{9–10}$ fragment by BCA protein assay (Pierce, Rockford, IL). Finally, reactive nanocarrier of various sizes and ligand-SH were incubated together at room temperature for 6 hours to conjugate the GST-FNIII$_{9–10}$ fragment to the surface of the carrier. Unreacted GST-FNIII$_{9–10}$ fragment was removed from the conjugation products by dialysis (MWCO 100 kDa).

Interfacial Characterization of GST-FNIII$_{9–10}$-Nanocarriers

Levels of GST-FNIII$_{9–10}$ conjugated to nanocarriers were quantified by enzyme-linked immunosorbent assay (ELISA) for GST and an ELISA for albumin was performed simultaneously for normalization of GST-FNIII$_{9–10}$ levels, both previously described by us.[22] Briefly, GST-FNIII$_{9–10}$-nanocarriers and standards of GST-FNIII$_{9–10}$ or albumin (Sigma) were adsorbed onto MaxiSorp 96 well plates (Nunc). Wells were blocked with 3% non-fat dry-milk, incubated with rabbit anti-GST (70 ng/mL) (Sigma) or horseradish peroxidase-conjugated rabbit anti-albumin (1:2500 dilution) (MP Biomedicals, Irvine, CA): wells incubated with anti-GST primary antibody were washed and further reacted with an appropriate horseradish peroxidase-conjugated goat anti-rabbit antibody (1:40,000) (Sigma). Sigma-FAST OPD tablets (Sigma) were used as a substrate for the detection of peroxidase activity by developing for 30 minutes and reading the absorbance at 450 nm on a multiwell plate reader. To examine the role of mobility of our ligand through differential presentation, ligand and ligand-nanocarriers were immobilized to the surface using oxygen plasma pretreatment (March Plasma Inc, 60 seconds, 50 W, 670 mTorr oxygen) before ligand and ligand-nanosubstrate deposition. Isotherms were established as described above.

ELISAs were also conducted to examine exposure of GST-FNIII$_{9–10}$ cell binding domains as a function of ligand nanodisplay for both passively adsorbed and immobilized substrates. Equivalent amounts of GST-FNIII$_{9–10}$ derived from GST ELISA isotherms were adsorbed on maxisorp 96 well plates overnight at 4°C. The surfaces were washed and blocked for 1 hour at 37°C. Substrates were washed again and incubated with the primary antibody specific for the cell-binding domain of fibronectin (Clone 3E3; Chemicon International, Temecula, CA) for one hour, followed by one hour incubation with horseradish peroxidase conjugated-goat anti-mouse IgG (Sigma). Peroxidase activity was detected as described above.

Cell Isolation and Culture

Human keratinocytes were isolated via enzyme digestion from neonatal foreskin as previously described by us.[22] Cells were cultured in keratinocyte growth medium (KGM) (Clonetics, San Diego, CA) containing 0.1 ng/ml epidermal growth factor (EGF), 5 μg/ml insulin, 0.5 μg/ml hydrocortisone, 50 μg/ml gentamicin, 50 ng/ml amphotericin-B, 0.15 mM calcium, and 30 μg/ml bovine pituitary extract (BPE). Cell passages 2 to 3 were utilized for all experimental studies. To fully define the culture media for experiments with ligand-nanocarriers, media was switched to KGM without BPE and EGF at least 16 hours prior to the experiment and during the experiment.

Cell Morphology

Labtek chamber slides (Nunc, Rochester, NY) were adsorbed overnight at 4°C with GST-$FNIII_{9–10}$ conjugated nanocarriers, net equivalents of GST-$FNIII_{9–10}$ fragment alone (as determined by ELISA), or unfunctionalized nanocarriers. Wells were washed three times, blocked as described above, and keratinocytes seeded at 8,000 cells per well. After a 5 hour incubation at 37°C, cells were washed with DPBS with calcium and magnesium, fixed in 3.7% formaldehyde (15 minutes), permeabilized with 0.5%Triton X-100 (15 minutes), and blocked with 1% normal goat serum/3% bovine serum albumin (15 minutes). Actin was labeled using fluorescein labeled phalloidin (1:200 dilution) (Molecular Probes). Cells were imaged using a Leica SP/2 Confocal Laser Scanning Microscope.

Cell Migration on Ligand versus various sized Ligand-Nanocarriers

Cell motility kinetics were investigated by seeding isolated keratinocytes at the concentration of 2800 cell/cm^2 on to wells coated with either ligand-nanocarriers, nanocarriers, or ligand overnight at 4°C. Wells were then washed three times with copious amounts of PBS and blocked with bovine serum albumin (1h, 37°C). Cells were seeded and then transferred to the microscope. Four non-overlapping viewing fields containing single cells were identified in each of the wells and continually imaged at 20× magnification under transmitted light for a total of 10 h at 15 minute intervals. Images were then analyzed with Image Pro Plus (Media Cybernetics, Silver Springs, MD). For each image, the x and y location of the cell centroid was recorded throughout each sequence of images and the mean square displacement of the cell tracks was computed for each time interval.

$$\langle d^2(t=n\Delta t)\rangle = \frac{1}{(N-n+1)}\sum_{i=0}^{N-n}[[x((n+i)\Delta t) - x(i\Delta t)]^2 + [y((n+i)\Delta t) - y(i\Delta t)^2] \quad (1)$$

Cell motility was quantified by modeling the cell motility behavior as a persistent random walk in an isotropic environment.[10] Briefly, the mean-squared displacement, given by

$$\langle d^2\rangle = 2S^2P[t - P(1 - e^{\frac{-t}{P}})] \quad (2)$$

is a function of time, with two major single cell motility parameters, root mean squared cell speed, S, and directional persistence time, P. Experimental data was used to fit the above equations and regress the best estimates for S, which were used to represent cell migration rates.

In the conditions exhibiting the highest levels of cell migration, surfaces were pretreated with oxygen plasma prior to incubation with FNf or FNf-nanocarriers to immobilize the ligands and examine the role of cellular internalization of ligands. To examine the role of various endocytic pathways on keratinocyte migrating on these interfaces, cells were pre-incubated with inhibitors of clathrin or caveolin mediated endocytic pathways. Briefly, keratinocytes were pre-incubated with either filipin (Sigma) at 5 μg/ml, to inhibit caveolin-mediated endocytosis, or chlorpromazine (Sigma) at 10 μg/ml, to inhibit clathrin-mediated endocytosis, prior to examining cell migration.[46]

Evaluation of JNK Expression by ELISA

Phosphorylated JNK activity was measured using a commercially available colorimetric ELISA (Biosource International). Substrates were prepared as described above, and cells were cultured for 3 hours before being lysed as per manufacturer's protocols with 10 mM Tris, pH 7.4, 100 mM NaCl, 1 mM EDTA, 1 mM EGTA, 1 mM NaF, 20 mM $Na_4P_2O_7$, 2

mM Na_3VO_4, 1% Triton X-100, 10% glycerol, 0.1% SDS, 0.5% deoxycholate, 1 mM PMSF (stock is 0.3 M in DMSO), protease inhibitor cocktail (Sigma). Lysates were collected and a BCA assay was performed to determine the protein concentration. As per the manufacturer's protocol, samples that were less than 2.5 mg/ml were boiled for 5 minutes. Samples and standards were adsorbed to wells precoated with a monoclonal antibody specific for JNK1/2, regardless of phosphorylation state. Samples were adsorbed overnight at 4°C. After washing with provided washing buffer, an antibody specific for JNK1/2 phosphorylated at threonine 183 and tyrosine 185 is added to the wells for 1 hour at room temperature. Another wash is performed, and during the second incubation, a horseradish peroxidase-labeled anti-rabbit IgG (anti-rabbit IgG-HRP) is added. After a third incubation and washing to remove all the excess anti-rabbit IgG-HRP, a substrate solution is added, which is acted upon by the bound enzyme to produce color. The standard curve was used to calculate the phosphorylated JNK activity by using the absorbance reading to determine the equivalent activity.

Uptake of Fluorescent Ligand-Nanocarriers

Internalized ligand-nanocarriers were quantitated using extracellular fluorescent quenching techniques described by others.[47] Fluorescent nanocarriers were prepared by denaturing albumin and adding fluorescein isothiocyanate (FITC) (Molecular Probes) at a stock concentration of 100 μg/ml at a ratio of 100 μl per 30 ml batch of nanocarriers. The solution was then stirred to form differentially sized nanocarriers and purified, functionalized and adsorbed on 96 well plates as described above. Keratinocytes were seeded at 10,000 cells per well in media supplemented with Trypan blue at a final concentration was 0.2%. As the trypan blue quenches extracellular fluorescence, degree of internalized fluorescent ligand-nanocarriers was quantified in terms of fluorescence intensity. Uptake was detected using a Cytofluor fluorescent plate reader (Applied Biosystems, CA) (excitation 485, emission 520) each hour for 6 hours. The amount of albumin taken up each hour was determined by normalizing the readings at each time point against the reading at 1 hour. The slope of the curve was used to estimate the rate of intensity increase. Uptake studies were also performed for immobilized substrates and cells cultured in the presence of endocytic inhibitors. Control conditions, including ligand-adsorbed substrates, media presented ligand-nanocarriers, and unfunctionalized substrates, were examined.

Supplementary Material

Refer to Web version on PubMed Central for supplementary material.

Acknowledgments

We gratefully acknowledge support of NSF NIRT: 0609000, NIH EB EB001046, NSF DGE 0333196, Rutgers University Academic Excellence Award (for PVM), and NIH GM059383 (for JES). RIS was supported by a Rutgers-UMDNJ National Institutes of Health Biotechnology Training Fellowship and Rutgers National Science Foundation IGERT fellowship. We also appreciate contributions from Dr. María Pía Rossi for editorial assistance, Dominik Naczynski for producing Figure 1, Thomas Gentzel, a recipient of a Rutgers-NSF IGERT Summer Undergraduate Research Fellowship, for image analysis; Rebecca Moore and Eileen Dawson for help with PCR protocols, and Nicolette Wangler at Princeton University for ligand purification.

References

1. O'Toole EA. Clin Exp Dermatol. 2001; 26:525. [PubMed: 11678882]
2. Godbey WT, Atala A. Ann N Y Acad Sci. 2002; 961:10. [PubMed: 12081857]
3. Auger FA, Berthod F, Moulin V, Pouliot R, Germain L. Biotechnol Appl Biochem. 2004; 39:263. [PubMed: 15154837]
4. Allen JW, Bhatia SN. Tissue Eng. 2002; 8:725. [PubMed: 12459052]
5. Lutolf MP, Hubbell JA. Nat Biotechnol. 2005; 23:47. [PubMed: 15637621]

6. Silva EA, Mooney DJ. Curr Top Dev Biol. 2004; 64:181. [PubMed: 15563948]
7. Nair LS, Bhattacharyya S, Laurencin CT. Expert Opin Biol Ther. 2004; 4:659. [PubMed: 15155157]
8. Friedl P, Zanker KS, Brocker EB. Microsc Res Tech. 1998; 43:369. [PubMed: 9858334]
9. Palecek SP, Loftus JC, Ginsberg MH, Lauffenburger DA, Horwitz AF. Nature. 1997; 385:537. [PubMed: 9020360]
10. DiMilla PA, Stone JA, Quinn JA, Albelda SM, Lauffenburger DA. J Cell Biol. 1993; 122:729. [PubMed: 8335696]
11. Goldstein AS, DiMilla PA. J Biomed Mater Res. 2002; 59:665. [PubMed: 11774328]
12. Burmeister JS, Vrany JD, Reichert WM, Truskey GA. J Biomed Mater Res. 1996; 30:13. [PubMed: 8788101]
13. Iuliano DJ, Saavedra SS, Truskey GA. J Biomed Mater Res. 1993; 27:1103. [PubMed: 8408123]
14. Sharma RI, Kohn J, Moghe PV. J Biomed Mater Res A. 2004; 69:114. [PubMed: 14999758]
15. Maheshwari G, Brown G, Lauffenburger DA, Wells A, Griffith LG. J Cell Sci. 2000; 113(Pt 10): 1677. [PubMed: 10769199]
16. Tjia JS, Moghe PV. Ann Biomed Eng. 2002; 30:851. [PubMed: 12220084]
17. Tjia JS, Moghe PV. Tissue Eng. 2002; 8:247. [PubMed: 12031114]
18. Lee K, Alsberg E, Hsiong S, Comisar W, Lindeman J, Ziff R, Mooney D. Nano Letters. 2004; 4:1501.
19. Ridley AJ, Schwartz MA, Burridge K, Firtel RA, Ginsberg MH, Borisy G, Parsons JT, Horwitz AR. Science. 2003; 302:1704. [PubMed: 14657486]
20. Caswell P, Norman J. Trends Cell Biol. 2008; 18:257. [PubMed: 18456497]
21. Sadowski L, Pilecka I, Miaczynska M. Exp Cell Res. 2008
22. Sharma RI, Pereira M, Schwarzbauer JE, Moghe PV. Biomaterials. 2006; 27:3589. [PubMed: 16527347]
23. Pereira M, Sharma RI, Penkala R, Gentzel TA, Schwarzbauer JE, Moghe PV. Tissue Eng. 2007; 13:567. [PubMed: 17518603]
24. Leahy DJ, Aukhil I, Erickson HP. Cell. 1996; 84:155. [PubMed: 8548820]
25. Main AL, Harvey TS, Baron M, Boyd J, Campbell ID. Cell. 1992; 71:671. [PubMed: 1423622]
26. Aota S, Nomizu M, Yamada KM. J Biol Chem. 1994; 269:24756. [PubMed: 7929152]
27. Obara M, Kang MS, Yamada KM. Cell. 1988; 53:649. [PubMed: 3286012]
28. Mould AP, Askari JA, Aota S, Yamada KM, Irie A, Takada Y, Mardon HJ, Humphries MJ. J Biol Chem. 1997; 272:17283. [PubMed: 9211865]
29. Mould AP, Askari JA, Humphries MJ. J Biol Chem. 2000; 275:20324. [PubMed: 10764748]
30. Redick SD, Settles DL, Briscoe G, Erickson HP. J Cell Biol. 2000; 149:521. [PubMed: 10769040]
31. Altroff H, Choulier L, Mardon HJ. J Biol Chem. 2003; 278:491. [PubMed: 12376529]
32. Kim JP, Zhang K, Chen JD, Wynn KC, Kramer RH, Woodley DT. J Cell Physiol. 1992; 151:443. [PubMed: 1295896]
33. Gao H, Shi W, Freund LB. Proc Natl Acad Sci U S A. 2005; 102:9469. [PubMed: 15972807]
34. Jiang W, Kim BY, Rutka JT, Chan WC. Nat Nanotechnol. 2008; 3:145. [PubMed: 18654486]
35. Chithrani BD, Ghazani AA, Chan WC. Nano Lett. 2006; 6:662. [PubMed: 16608261]
36. Bishop AL, Hall A. Biochem J. 2000; 348(Pt 2):241. [PubMed: 10816416]
37. Kirfel G, Herzog V. Protoplasma. 2004; 223:67. [PubMed: 15221512]
38. Kirfel G, Rigort A, Borm B, Schulte C, Herzog V. Cell Motil Cytoskeleton. 2003; 55:1. [PubMed: 12673594]
39. Huang C, Jacobson K, Schaller MD. J Cell Sci. 2004; 117:4619. [PubMed: 15371522]
40. Huang C, Rajfur Z, Borchers C, Schaller MD, Jacobson K. Nature. 2003; 424:219. [PubMed: 12853963]
41. Huang Z, Yan DP, Ge BX. Cell Signal. 2008; 20:2002. [PubMed: 18713649]
42. Vaslin A, Puyal J, Borsello T, Clarke PG. J Neurochem. 2007; 102:789. [PubMed: 17437546]
43. Cui Q, Tashiro S, Onodera S, Minami M, Ikejima T. J Pharmacol Sci. 2007; 105:317. [PubMed: 18094523]

44. Panicker AK, Buhusi M, Erickson A, Maness PF. Exp Cell Res. 2006; 312:299. [PubMed: 16330023]

45. Pierini LM, Lawson MA, Eddy RJ, Hendey B, Maxfield FR. Blood. 2000; 95:2471. [PubMed: 10753823]

46. Rejman J, Oberle V, Zuhorn IS, Hoekstra D. Biochem J. 2004; 377:159. [PubMed: 14505488]

47. Su M, He C, West CA, Mentzer SJ. J Immunol Methods. 2001; 252:63. [PubMed: 11334966]

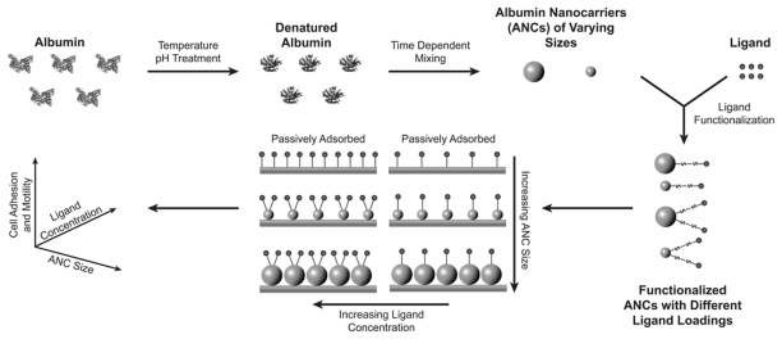

Figure 1.

Schematic summarizing the experimental design of biofunctionalized albumin-derived nanocarriers (ANCs). ANCs were fabricated by self-assembly of recombinant human serum albumin following denaturation via changes in pH and temperature. The suspension was stirred for various times to yield differentially sized carriers, the self-assembly was terminated, and purified. Variably sized ANCs were conjugated with ligand (GST-FNIII9–10) and biofunctionalized ANCs were adsorbed at different concentrations to yield substrates with differing nanocarrier sizes and ligand concentrations. This experimental system was used to probe cell adhesion, migration, and intracellular uptake and biochemical signaling responses.

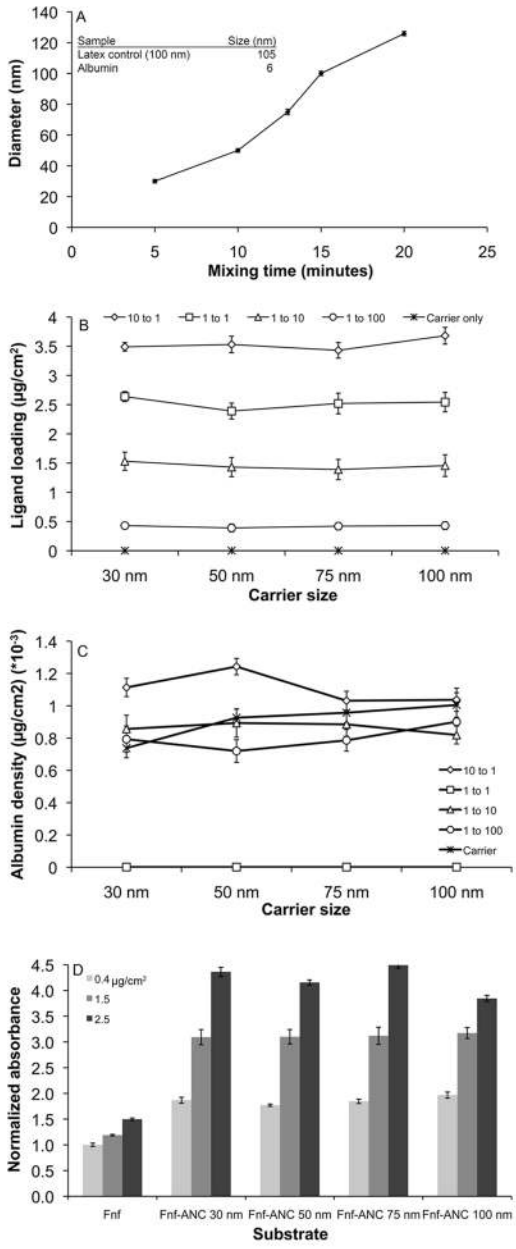

Figure 2.

(A) Differential nanoscale sizing of albumin derived nanocarriers (ANCs). Nanocarrier sizes at different stirring times were confirmed using dynamic light scattering (DLS). Inset: DLS readings for latex control and monomeric albumin. (B) Ligand-conjugated ANCs were characterized for the range of ligand (GST-FNIII9–10) presented. The mass of ANCs was held constant (400 μg) and increasing amounts of ligand were functionalized on various sized carriers and quantified by ELISA for GST. (C) Ligand presentation from ANCs of different sizes. GST ligand levels were normalized to albumin quantified via ELISA on respective conditions. (D) The exposure of cell binding domains was analyzed using ELISA for Clone 3E3 fibronectin based on ligand density and nanocarrier size. Results represent average of three experiments performed in duplicate with the standard error plotted around the mean.

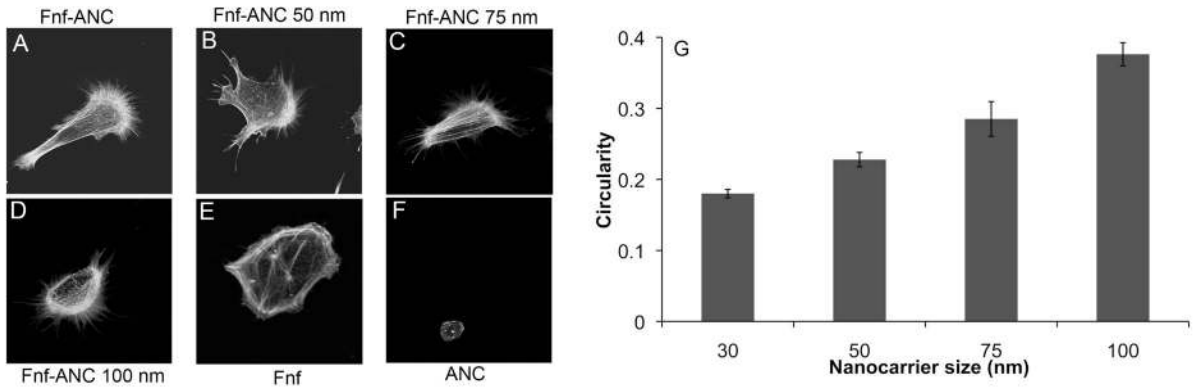

Figure 3.

(A–D) Ligand-nanocarriers induce filopodial microextensions in primary human keratinocytes indicative of a motile phenotype, in contrast to a stationary phenotype seen on ligand controls (E) and the rounded, unresponsive phenotype on unfunctionalized ANC substrates (F). Substrates were prepared by adsorbing equivalent ligand concentrations of ligand-nanocarriers or ligand-adsorbed controls as described in the text. Serum-starved cells were fixed, permeabilized, and labeled for F-actin with FITC-phalloidin. Cells cultured on functionalized nanocarriers display filopodia around the cell. (G) Cell morphological polarity was quantified as a function of biofunctionalized ANCs of different sizes. The circularity is a ratio of the cell area to the squared perimeter. Data indicates that cells become more polarized on smaller ligand-functionalized nanocarriers, and conversely adopt a more rounded morphology when cultured on larger-sized nanocarriers functionalized with ligand.

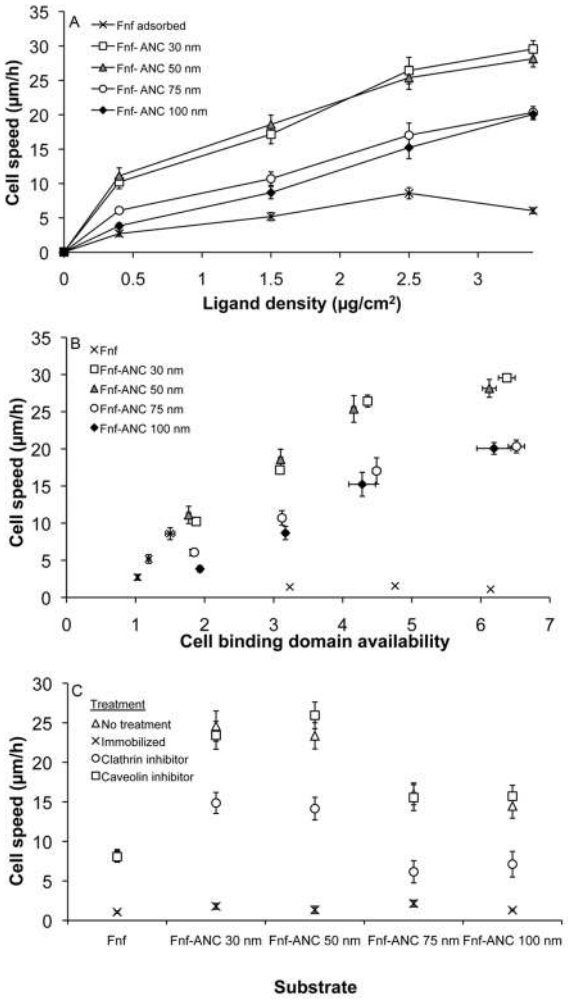

Figure 4.

(A) Single keratinocyte cell migration was quantified on substrates adsorbed with ligand alone, nanocarriers alone, and ligand-conjugated nanocarriers over a range of varying ANC sizes and ligand concentrations. Data represents the average of all data from 3 experiments performed in duplicate. For each experiment, n=60 tracks. Error bars represent standard error around the mean. At comparable net levels of ligands presented, the smaller sized nanocarriers (30nm) elicited higher levels of cell motility than the larger sized nanocarriers (100nm). (B) We examined whether the effects of ANC carriers on cell migration were due to the differential exposure and bioactivity of ligands from nanocarriers of different sizes. ELISA techniques were used to quantify the exposure of cell binding domains of the nanocarrier-functionalized type III-9–10 fibronectin fragment. While increased ligand bioactivity (cell binding domain exposure) generally correlated with increased cell migration speed, it did not uniquely govern cell speeds; additionally, geometric (size) aspects of ANCs additionally modulated cell migration. (C) The role of ligand-nanocarrier endocytosis on cell migration was examined by comparing cell migration on physisorbed ligand-ANC ("passive" condition) versus ligand-ANCs controls chemically immobilized via oxygen plasma treatment of well plates. Cells were pretreated with either filipin (caveolin inhibitor) or chlorpromazine (clathrin inhibitor) before deposition on passively adsorbed substrates. Images were acquired and analyzed as described above. Cell migration on physisorbed ligand-ANCs was significantly enhanced in comparison to that on immobilized substrates.

Inhibition of clathrin but not caveolin reduced levels of cell migration indicating a key role for clathrin mediated endocytosis.

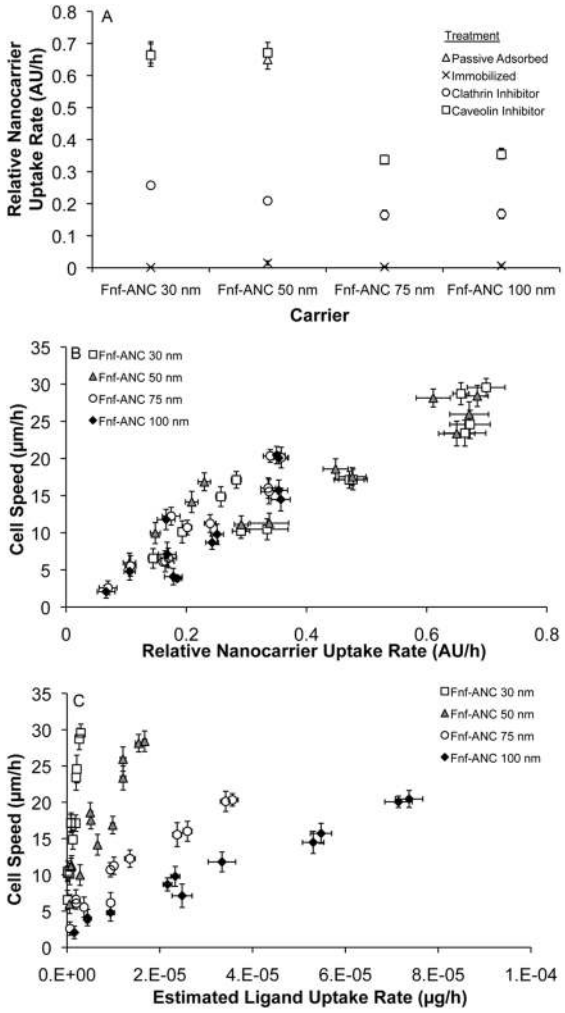

Figure 5.

(A) The role of ligand-nanocarrier endocytosis was directly confirmed and quantified at various nanocarrier sizes and following treatment with endocytic inhibitors. Briefly, fluorescent nanocarriers were prepared by denaturing albumin and incorporating the fluorophore FITC prior to self-assembly, and functionalized with ligand as described in the text. Well plates were adsorbed with various sized ligand-nanocarriers, while control wells were treated with oxygen plasma to immobilize ligand-nanocarriers. Cells or cells pretreated with inhibitors of caveolin or clathrin were deposited on substrates and trypan blue was added to the media for 1 hour prior to detection (excitation 485 nm, emission 520 nm). Fluorescent intensity readings were taken at regular intervals, plotted, and the rate of intensity increase was determined. Uptake studies showed that the rate of uptake was greater for 30 and 50 nm sized nanocarriers, and lower for 75 and 100 nm sized nanocarriers. Ligand-nanocarrier uptake in cells was inhibited by clathrin inhibitors but not by caveolin inhibitors. Immobilized controls showed minimal uptake. (B) Cell migration data from various experimental conditions (physically adsorbed substrates, immobilized substrates, and endocytic inhibition) were aggregated and plotted against respective uptake experimental data. (C) The theoretical ligand coverage on each nanocarrier was estimated (see supplementary text), factored into the nanocarrier uptake rate to determine the ligand uptake rate and plotted against the cell speed from various experiments. The degree of

ligand uptake differentially correlates with cell migration rate, governed by the nanocarrier size.

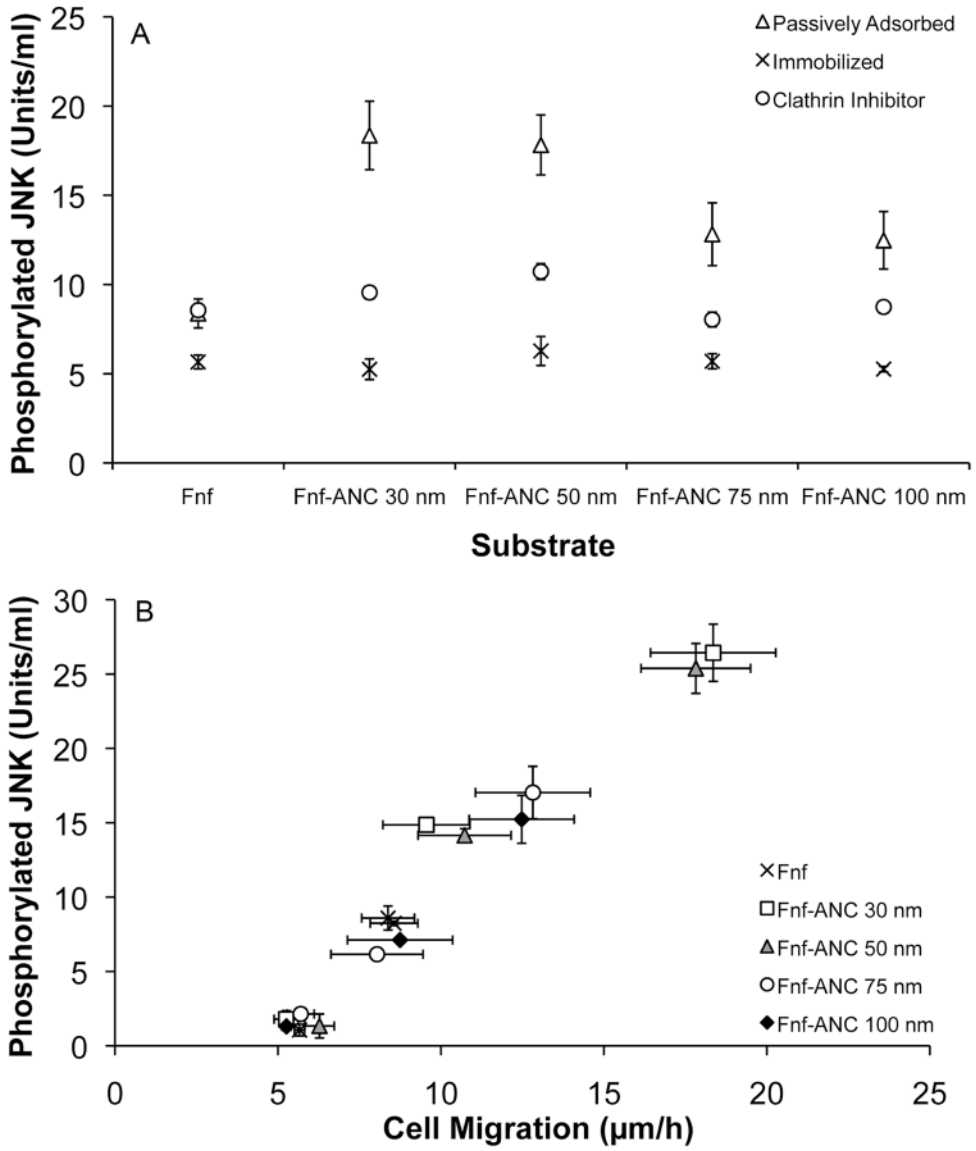

Figure 6.

(A) The activity of phosphorylated JNK (P-JNK), one of the key intracellular signaling molecules, was examined for keratinocytes cultured on ligand-nanocarriers of varying sizes either physically adsorbed or immobilized via plasma treatment. P-JNK Activity was enhanced on smaller nanocarriers that were physically adsorbed. Untreated cells or control cells pretreated with inhibitors of clathrin mediated endocytosis were deposited on substrates, lysed, and protein concentration determined. Equal masses of protein were incubated in well plates that were preadsorbed with a primary antibody for JNK. Substrates were washed and a primary antibody specific for phosphorylated JNK was added to the wells. Levels were detected using a secondary with horseradish peroxidase conjugated to it. (B) Phosphorylated JNK activity correlates well with overall cell migration rate indicating that the adhesion and endocytosis events underlying cell migration coordinate activation across a wide range of conditions.